Supplementary Materials for

A human apolipoprotein L with detergent-like activity kills intracellular pathogens

Ryan G. Gaudet, Shiwei Zhu, Anushka Halder, Bae-Hoon Kim, Clinton J. Bradfield, Shuai Huang, Dijin Xu, Agnieszka Mamiñska, Thanh Ngoc Nguyen, Michael Lazarou, Erdem Karatekin, Kallol Gupta, John D. MacMicking*

*Corresponding author. Email: john.macmicking@yale.edu

Published 16 July 2021, *Science* **373**, eabf8113 (2021)
DOI: 10.1126/science.abf8113

This PDF file includes:

Other supplementary material for this manuscript includes:

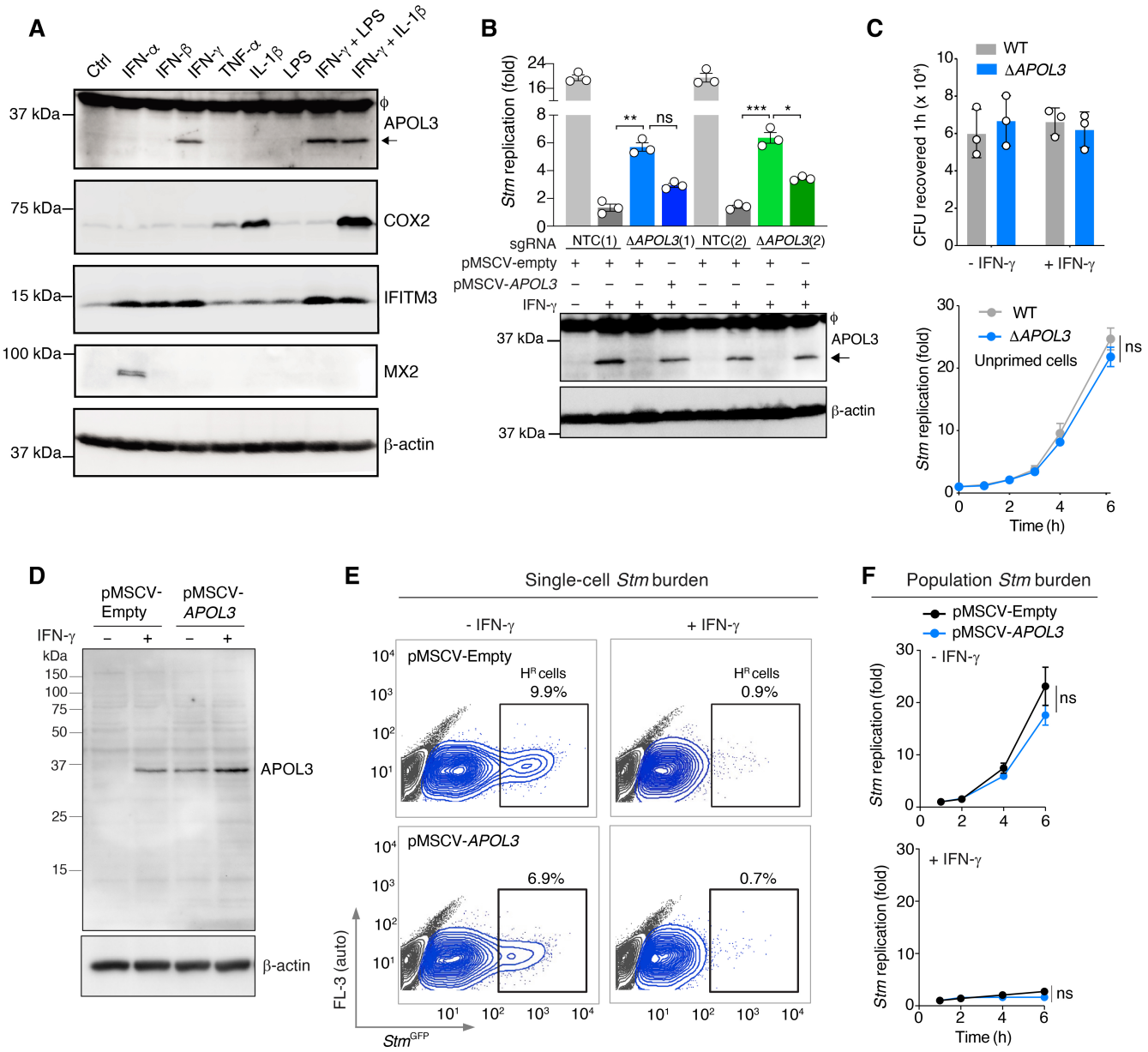

Fig. S1. APOL3 is an IFN-γ-stimulated gene that exerts antibacterial effects within activated cells. (**A**) HeLa cells stimulated as indicated for 18 h and whole cell lysates probed by immunoblot. Concentrations used: IFN-α/β/γ (500 U/ml), TNFα (100 ng/ml), IL-1β (10 ng/ml), LPS (10 μg/ml). MX2 (MX Dynamin like GTPase 2), COX2 (Cyclooxygenase-2) and IFITM3 (Interferon Induced Transmembrane Protein 3) were blotted as positive controls. (**B**) HeLa cells of the indicated genotype complemented with *APOL3* (or empty control) encoded within a pMSCV retroviral construct were treated with IFN-γ for 18 h before being infected with *Stm* and intracellular growth measured after 6 h (relative to 1 h) by gentamicin protection assay. Whole cell lysates were probed by immunoblot. NTC represents a non-targeting control sgRNA, with multiple single cell clones [(1), (2)] selected for analysis. (**C**) Bacterial uptake measured by recovery of intracellular *Stm* from wildtype or Δ*APOL3* HeLa cells after 1 h (top) and time course of intracellular *Stm* growth by gentamicin protection assay in unprimed wildtype or Δ*APOL3* HeLa cells (below). (**D** to **F**), Effect of forced ectopic expression of pMSCV-*APOL3* on *Stm* replication

in wildtype HeLa cells (+/-) IFN-γ at the single-cell FACS at 6 h (E) and population (gentamicin protection assay) levels (F). Resulting APOL3 protein levels by immunoblot are shown in (D). Blots and FACS plots are representative of 3 or 4 independent experiments. Infected and non-infected cells are depicted in blue and gray respectively. Data are mean ± s.e.m from 3 independent experiments [(B), (C) and (F)] with significance determined by two-tailed *t*-test [(C) and (F)] or one-way ANOVA (B): ** $P< 0.01$, *** $P< 0.001$, ns, not significant. ϕ, non-specific band.

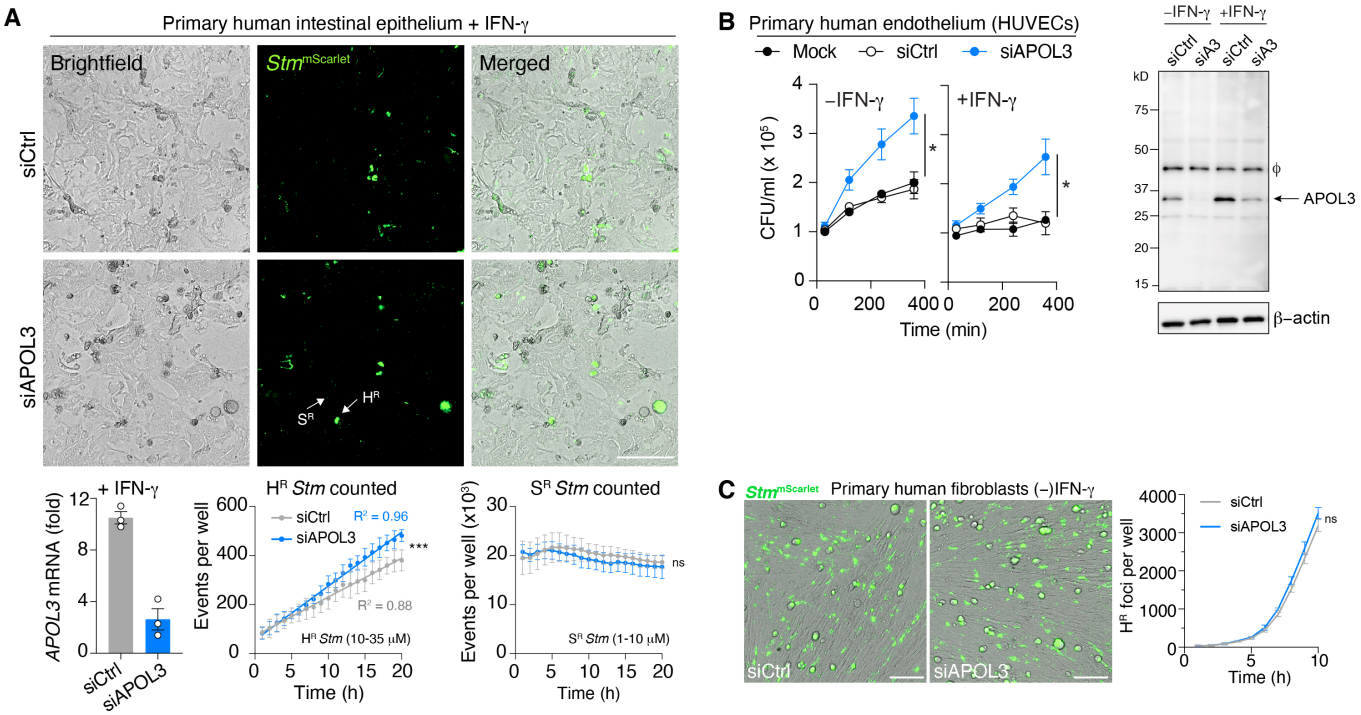

Fig. S2. An essential role for APOL3 in antibacterial defense of primary cells. (**A**) Micrographs of IFN-γ activated (50 U/ml) human primary intestinal epithelial cells treated with APOL3-targeting or non-targeting control siRNA and infected with *Stm*^{mScarlet} for 20 h. Below is quantification of *APOL3* mRNA by qPCR (left) and the number of H^R (10-35 μm) or S^R (1-10 μm) *Stm* foci counted (per well of a 96 well plate) over time. Data are mean ± s.d (n = 3) and are representative of 2 independent experiments. Growth curves were analyzed by simple linear regression with P value (***$P < 0.001$) comparing relative slope. (**B**) *Stm* replication measured by gentamicin protection assay in primary human umbilical vein endothelial cells (HUVEC) +/- IFN-γ (50 U/ml) treated with *APOL3* or control (Ctrl) siRNA. Diminished siRNA-induced APOL3 protein levels by immunoblot is below. (**C**) Micrographs of unprimed human primary intestinal myofibroblasts cells treated with APOL3-targeting or non-targeting control siRNA and infected with *Stm*^{mScarlet} for 10 h. Right is quantification of the number of H^R *Stm* foci (per well of a 96 well plate) over time. Data are mean ± s.e.m from 3 independent experiments [(B) and (C)]. * $P < 0.05$ by one-way ANOVA. ϕ, non-specific band. Arrow indicates APOL3 on immunoblot. Scale bars 75 μm.

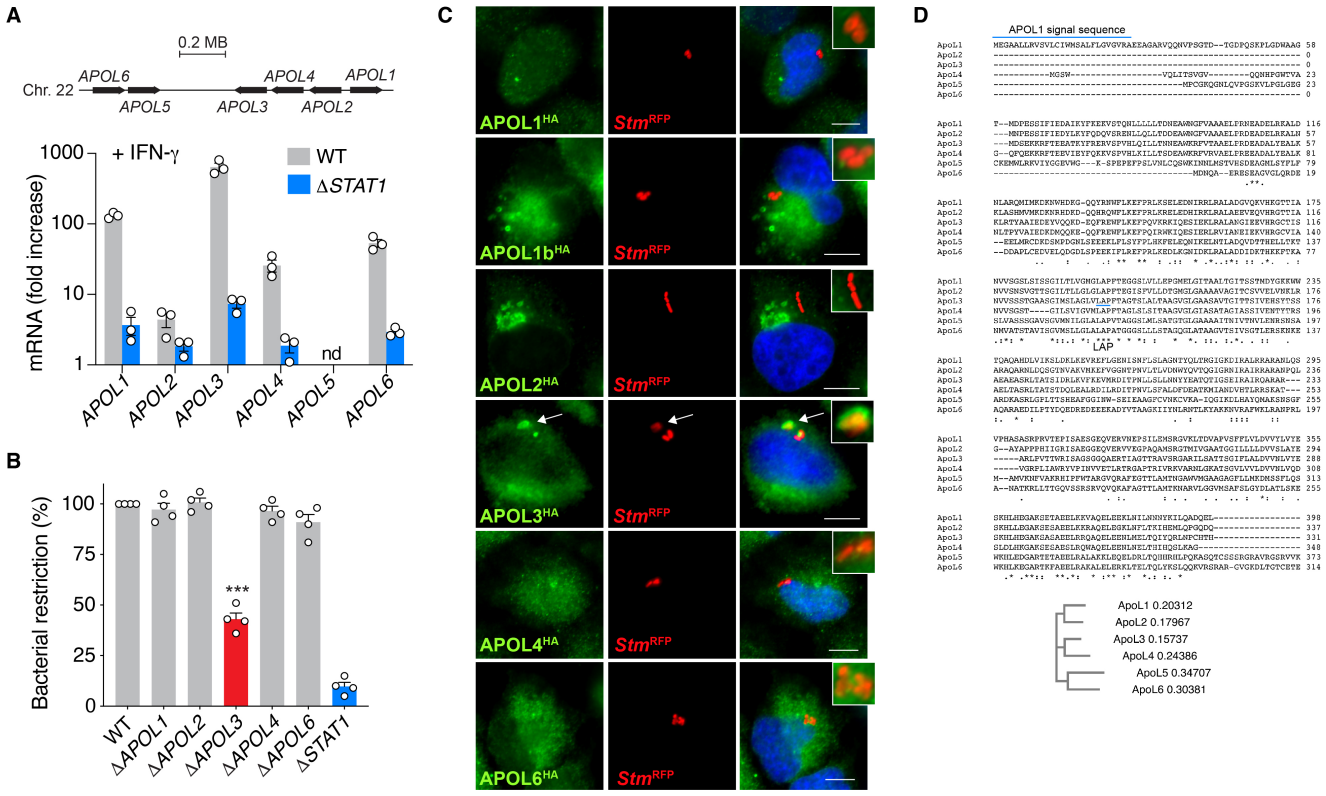

Fig. S3. Family wide analysis of the human *APOL* gene cluster. (**A**) Genome organization of the human *APOL* family clustered on chromosome 22 (Chr. 22) and qRT-PCR analysis (below) depicting fold induction of each *APOL* transcript after treatment with IFN-γ (500 U/ml) for 18 h in HeLa cells of the indicated genotype. (**B**) CRISPR-Cas9 deletion of each human *APOL* family member and its corresponding effect on IFN-γ-dependent restriction of intracellular *Stm* proliferation for 6 h (relative to WT). (**C**) Immunofluorescence analysis of pMSCV-HA-*APOL* family members (green) after infection with *Stm*^{RFP} for 2 h. *APOL1b* lacks the signal sequence of wildtype *APOL1* and is thus intracellular. Images are representative of 3 independent experiments. **(D)** ClustalW alignment and phylogeny of the human APOL protein family. Locations of the APOL1 signal peptide and the hydrophobic LAP patch are indicated. Micrographs are representative of 3 independent experiments. nd = not detected. Data are mean ± s.e.m from 3 (A) or 4 (B) independent experiments. *** $P < 0.001$ by ANOVA. Scale bar 5 μm.

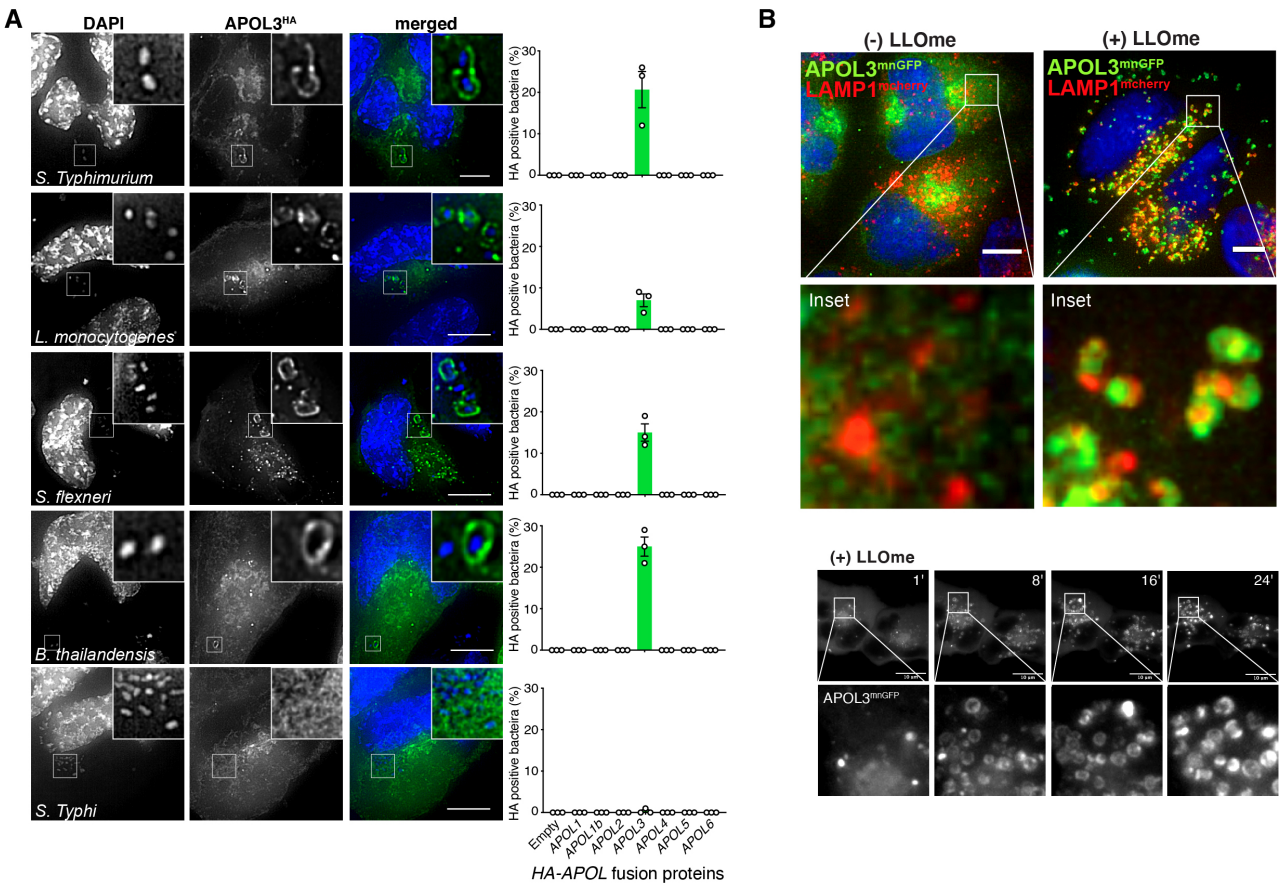

Fig. S4. APOL3 targets multiple cytosol-invasive bacteria by detecting host membrane damage. (**A**) Deconvolved widefield images of APOL3^{HA} during infection with *Salmonella enterica* serovar Typhimurium (1.5 h), *Listeria monocytogenes* (1.5 h), *Shigella flexneri* (1.5 h), *Burkholderia thailandensis* (3 h), and *Salmonella enterica* serovar Typhi (2 h). Bacteria are identified by DAPI (DNA). n = 50 bacteria counted per condition. Data are mean ± s.e.m from 3 independent experiments. (**B**) Deconvolved widefield images of HeLa cells expressing APOL3^{mnGFP} and Lamp1^{mCherry} pulsed with vehicle or the lysosomotropic agent L-leucyl-L-leucine methyl ester LLOme for 15 min (top). Below is time lapse images of a live APOL3^{mnGFP} expressing HeLa cell after addition of LLOme (min). Scale bars 5 μm.

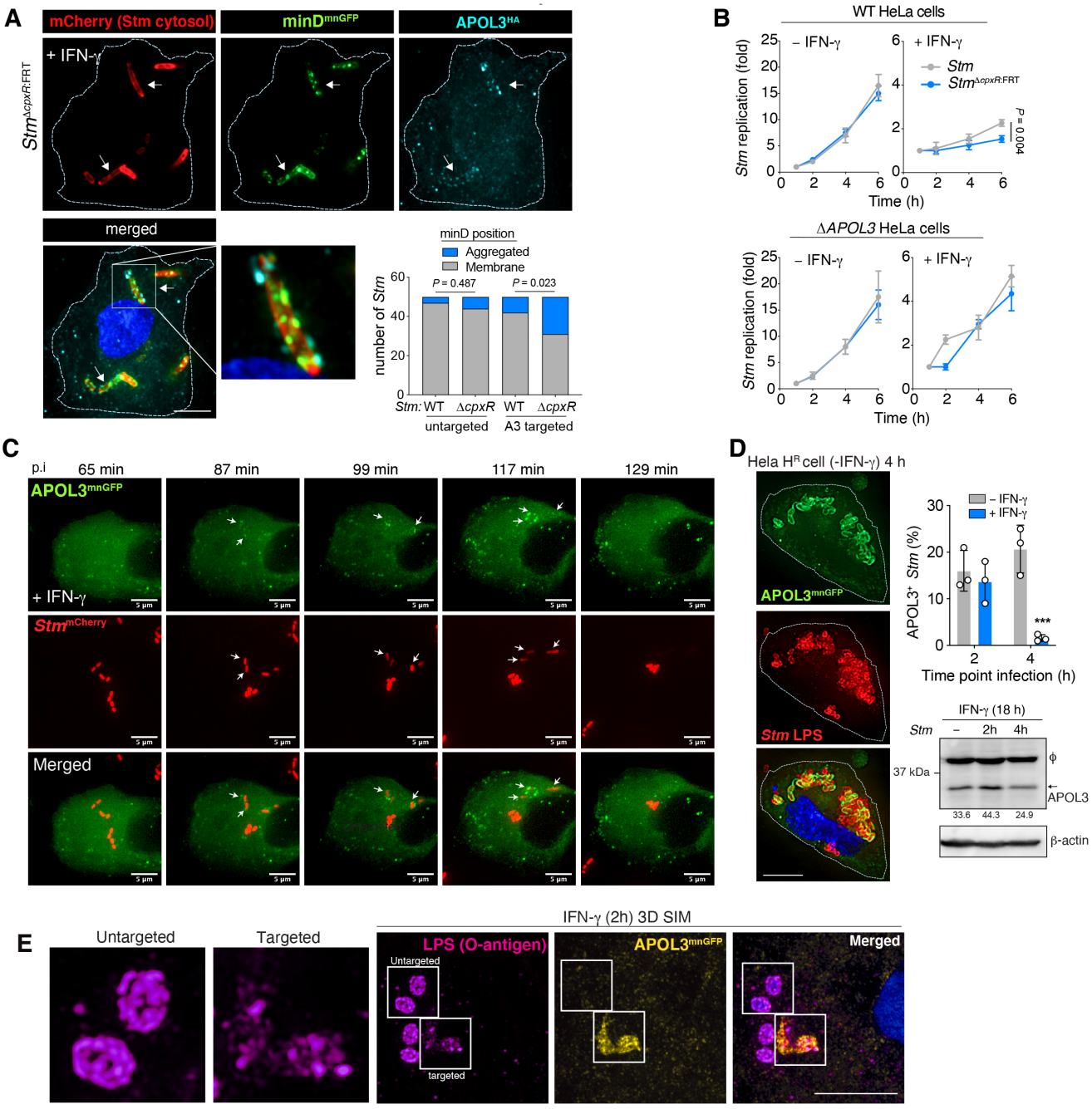

Fig. S5. Inner membrane disrupting activity of APOL3 inside IFN-γ-activated cells. (**A**) Deconvolved widefield images of *Stm*$^{\Delta cpxR:\mathrm{FRT}}$ *e*xpressing cytosolic mCherry and minD$^{\mathrm{mnGFP}}$ in Δ*APOL3* HeLa cells expressing HA-APOL3 2.5 h post infection. Aggregated or membrane-bound minD$^{\mathrm{mnGFP}}$ were enumerated (n = 50 per condition) in the presence of IFN-γ. (**B**) Growth of wildtype or *Stm*$^{\Delta cpxR:\mathrm{FRT}}$ in HeLa cells of the indicated genotype (+/-) IFN-γ (500 U/ml). (**C**) Time lapse widefield images of *Stm*$^{\mathrm{mcherry}}$ after infecting HeLa cells expressing APOL3$^{\mathrm{mnGFP}}$ in the presence of IFN-γ (500 U/ml). Targeted and cleared bacteria are indicated by arrows. (**D**) Deconvolved widefield image of an unprimed Δ*APOL3* hyper-replicating (H$^{\mathrm{R}}$) cell expressing

APOL3^{mnGFP} at 4 h p.i. *Stm* detected with anti-LPS antibody. Right is quantification of APOL3 positive *Stm* and APOL3 protein levels in whole-cell lysates by immunoblot 2 and 4 h post infection. (**E**) 3D SIM projections of *Stm* LPS (O-antigen specific antibody) and APOL3^{mnGFP} 2 h after infecting IFN-γ activated HeLa cells. Insets depict cytosol-exposed *Stm* (APOL3 targeted) that exhibit irregular O-antigen staining compared to vacuolar (untargeted). Data from [(A), (C), (D) and (E)] are representative of >3 independent experiments and enumerations in [(B) and (D)] are mean ± s.e.m from 3 independent experiments.Timelapse images in (B) were extracted from movie S6. Significance Fischer's exact test (A), unpaired *t*-test (B) or one-way ANOVA (D). *** $P < 0.001$. ϕ, non-specific band. Scale bar 5 μm.

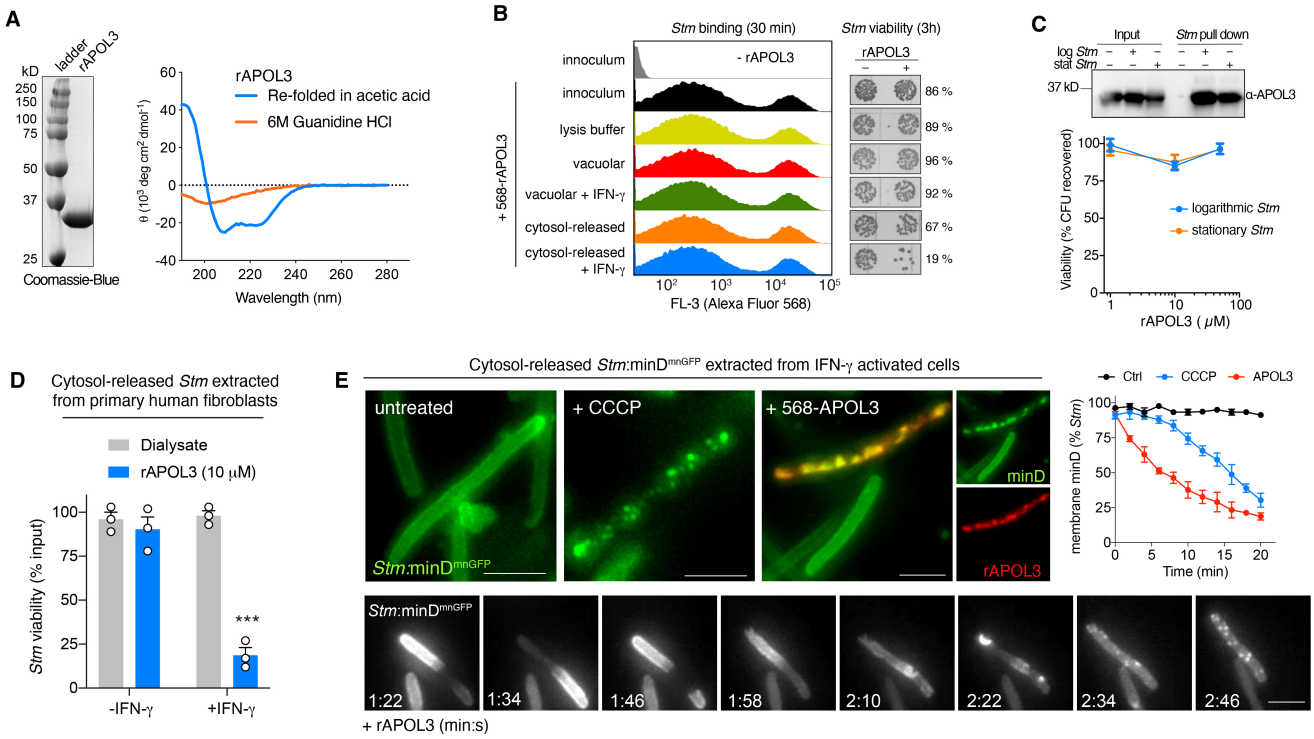

Fig. S6. Rapid *Stm* binding and membrane dysfunction triggered by APOL3. (**A**) Purification and re-folding recombinant APOL3. Coomassie blue staining after His-tag removal and re-folding from *E. coli* inclusion bodies by dialysis versus acetic acid (left). Re-folding was assessed by circular dichroism (right). (**B**) FACS histograms of *Stm* released with detergent from different compartments of Δ*APOL3* HeLa cells incubated with 568-labelled rAPOL3 for 30 min reveal equal amounts of bacterially bound APOL3. These bound fractions were incubated for an additional 3 h before plating for bacterial viability (right). (**C**) Binding and killing activity of rAPOL3 against logarithmic or stationary phase *Stm*. Bacterial viability determined 3 h after rAPOL3 exposure with increasing dosage. rAPOL3 binding assessed by bacterial pull-down and immunoblotting for APOL3. (**D**) Viability of *Stm* released into the cytsosol with LLOMe and extracted from primary human intestinal myofibroblasts (+/-) IFN-γ (50 U/ml) and treated with rAPOL3 for 2 h. (**E**) Validating minD^{mnGFP} aggregation in cytosol-released *Stm* extracted with detergent from Δ*APOL3* IFN-γ primed cells. Bacteria were exposed to CCCP (positive control) or 568-labelled rAPOL3 (5 μM) and imaged via wide-field microscopy. Micrographs at 10 min p.i. (top) or immediately after rAPOL3 addition (below). Data from [(A) to (C)] are representative of 2 independent experiments with enumerations in (C) mean ± s.d, *n*= *3*, or depicted as mean ± s.e.m from 3 independent experiments (D), or representative images and quantification [mean ± s.d from 3 technical replicates (*n* = 100 bacteria)] from one experiment out of three (E). *P* values by one-way ANOVA, *** $P < 0.001$. Scale bar, 2 μm.

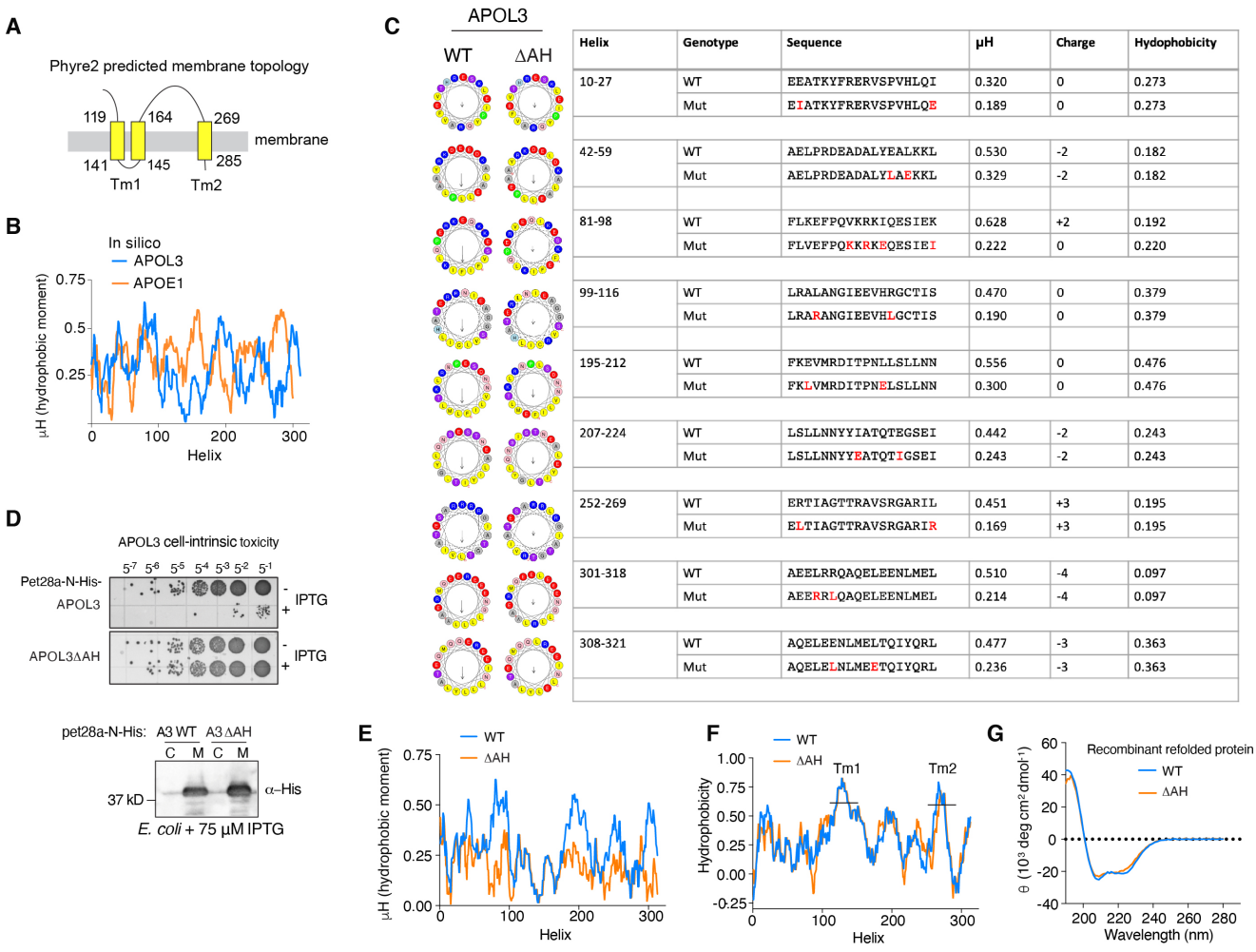

Helix	Genotype	Sequence	μH	Charge	Hydophobicity
10-27	WT	EEATKYFRERVSPVHLQI	0.320	0	0.273
	Mut	EIATKYFRERVSPVHLQE	0.189	0	0.273
42-59	WT	AELPRDEADALYEALKKL	0.530	-2	0.182
	Mut	AELPRDEADALYLAEKKL	0.329	-2	0.182
81-98	WT	FLKEFPQVKRKIQESIEK	0.628	+2	0.192
	Mut	FLVEFPQKKRKEQESIEI	0.222	0	0.220
99-116	WT	LRALANGIEEVHRGCTIS	0.470	0	0.379
	Mut	LRARANGIEEVHLGCTIS	0.190	0	0.379
195-212	WT	FKEVMRDITPNLLSLLNN	0.556	0	0.476
	Mut	FKLVMRDITPNELSLLNN	0.300	0	0.476
207-224	WT	LSLLNNYYIATQTEGSEI	0.442	-2	0.243
	Mut	LSLLNNYYEATQTIGSEI	0.243	-2	0.243
252-269	WT	ERTIAGTTRAVSRGARIL	0.451	+3	0.195
	Mut	ELTIAGTTRAVSRGARIR	0.169	+3	0.195
301-318	WT	AEELRRQAQELEENLMEL	0.510	-4	0.097
	Mut	AEERRLQAQELEENLMEL	0.214	-4	0.097
308-321	WT	AQELEENLMELTQIYQRL	0.477	-3	0.363
	Mut	AQELELNLMEETQIYQRL	0.236	-3	0.363

Fig. S7. ***In silico*** **analysis of APOL3 bactericidal activity.** (**A**) Predicted APOL3 membrane topology using Phyre2. (**B**) Hydrophobic moment (μH = amphipathicity) of APOL3 determined by HeliQuest with the canonical extracellular apolipoprotein APOE1 shown for comparison. (**C**) Helical wheel diagrams of predicted APOL3 amphipathic α-helices and engineered mutant (ΔAH). Swapped hydrophilic and hydrophobic amino acids (red) within each helix are shown along with the corresponding physiochemical properties for the ΔAH mutant (mut). (**D**) Cytotoxicity of APOL3 WT or ΔAH mutant (C) when overexpressed in *E. coli* via 75 μM IPTG overnight induction. Results are representative of 3 independent experiments. Subcellular location of toxicity shown by inducing His-APOL3 for 2 h and harvesting cytosolic (C) or membrane (M) fractions for immunoblot. (**E** to **G**) The hydrophobic moment (E), the hydrophobicity including each Tm region (F), and the observed secondary structure of re-folded recombinant protein as determined by circular dichroism (G) are shown for both wildtype and ΔAH APOL3. CD spectra is representative of 2 independent experiments.

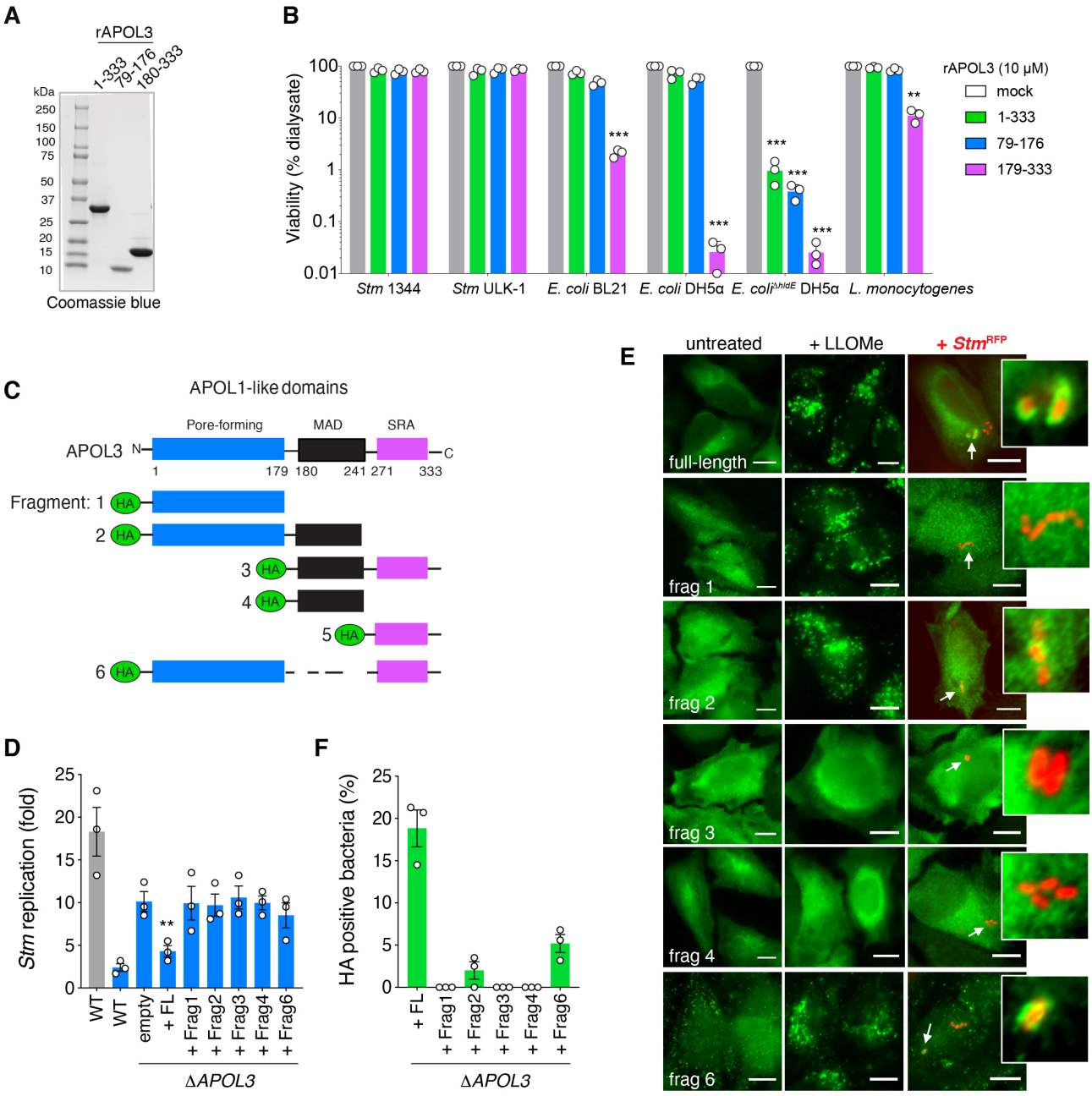

Fig. S8. Bactericidal activity of APOL3 fragments. (**A**) Coomassie-stained protein gels following purification of full-length (1-333) or the indicated rAPOL3 fragments after His-tag digestion and removal. (**B**) Viability of the indicated bacterial strain (log-phase) treated with rAPOL3 fragments (10 µM) for 3 h. Viability was determined by colony counting and normalized to dialysate treatment (mock). (**C**) Domains of human APOL3 based on sequence alignment with human APOL1 that contains a putative N-terminal pore-forming (ion channel) domain; membrane addressing domain (MAD); and C-terminal SRA domain by virtue of being targeted by the *Trypanosoma brucei rhodesiense* serum resistance-associated protein 27. (**D**) Replication of *Stm* at 6 h following genetic complementation of IFN-γ-activated (500 U/ml) Δ*APOL3* HeLa cells with retrovirally expressed APOL3 domains. (**E** and **F**) Immunofluorescence of HA-APOL3 domains

in untreated cells, after sterile membrane damage (LLOMe), or after infection with *Stm*^{RFP} (2 h). Fragment 5 was not expressed at detectable levels. Quantification of *Stm* targeting (n = 100 bacteria) is depicted in (F). Significance by one-way ANOVA: ** $P < 0.01$, *** $P < 0.001$. Results are ± s.e.m from 3 independent experiments. Scale bar 5 μm.

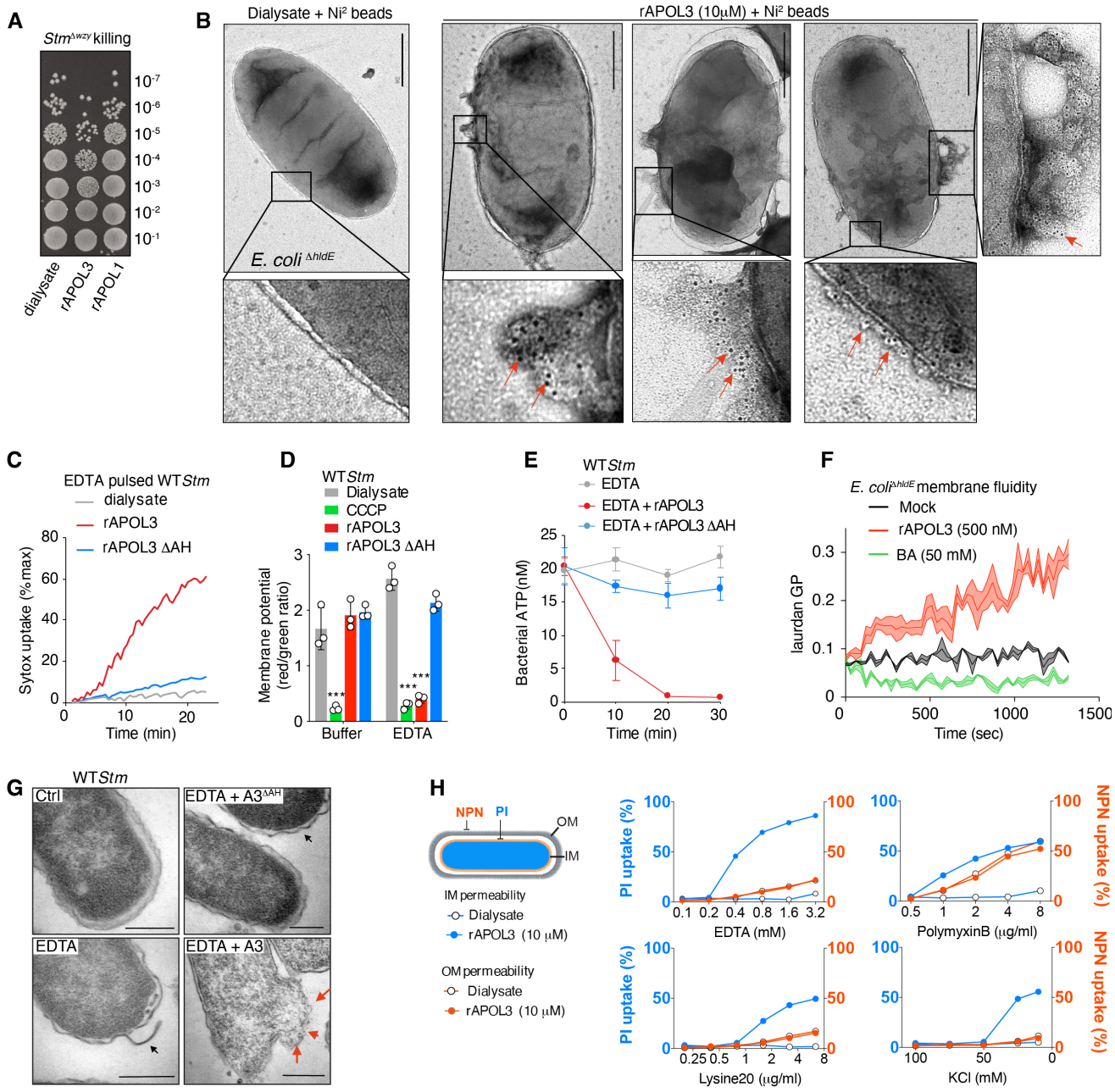

Fig. S9. APOL3 induces membrane lysis and dysfunction. (**A**) Viability of *Stm*$^{\Delta wzy}$ 3 h after treatment with dialysate, rAPOL3 or rAPOL1 (10 μM) at pH 5.5 in 0.15 M potassium gluconate. (**B**) Negative-stain EM of *E. coli*$^{\Delta hldE}$ exposed to His-APOL3 (or dialysate) for 5 min and detected with 5 nm Ni^{2+}-gold beads (arrows). (**C** to **E**) Time course of bacterial inner membrane (IM) permeability by Sytox ™ orange uptake (C), membrane potential at 2 h post-treatment (D) or intracellular ATP (E) of EDTA-pulsed *Stm* treated with wildtype or ΔAH rAPOL3. (**F**) *E. coli*$^{\Delta hldE}$ exposed to rAPOL3 (0.5 μM) and membrane fluidity measured with the fluorescent dye laurdan. High laurdan generalized polarization (GP) correlates with low membrane fluidity. Benzyl alcohol (BA) is a membrane fluidizer. (**G**) Transmission electron microscopy (TEM) of EDTA-pulsed *Stm*

30 min after addition of rAPOL3. Arrows indicate OM ruffling (black) or cytoplasmic leakage (red). (**H**) Outer membrane (OM) permeability of *Stm* measured by NPN uptake and IM permeability measured by PI uptake. *Stm* were treated with permeabilizing agents for 15 min then rAPOL3 or dialysate for 15 min and PI and NPN fluorescence measured. PI uptake normalized to 25 μg/ml polymyxin B (100%); NPN uptake normalized to 5 mM EDTA and 10 μg/ml lysozyme (100%). Data are mean ± s.e.m from 3 independent experiments [(D) and (E)], as means ± s.d from 3 replicates representative of 3 independent experiments (F) or single experiments representative of 2 to 3 biological replicates [(A), (B), (C) (G), (H)]. *** $P < 0.01$ by one-way ANOVA. Scale bars 500 nm (B), 200 nm (G).

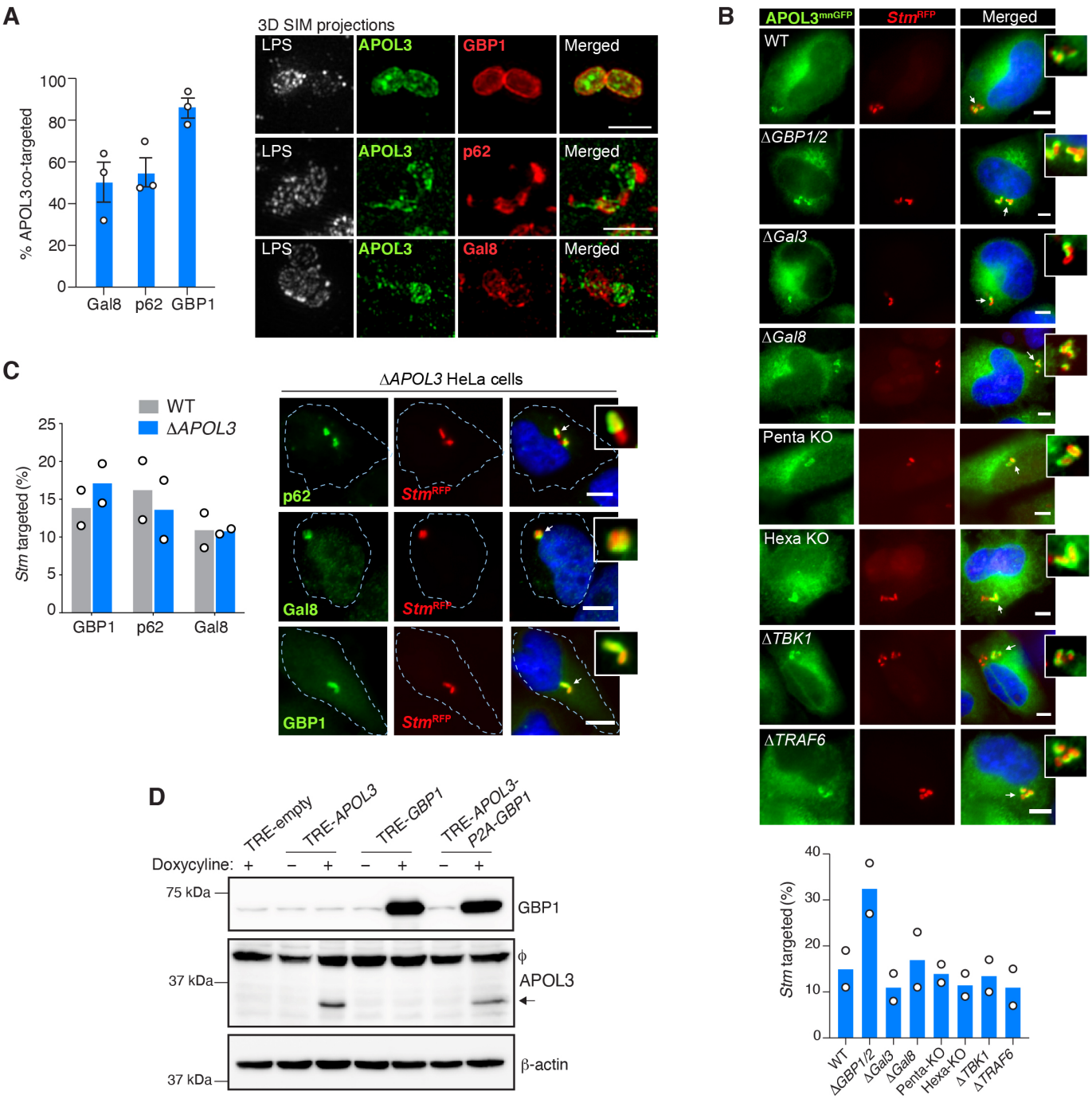

Fig. S10. Integration of APOL3 within canonical bacterial restriction pathways. (**A**) Immunofluorescence and 3D SIM projections of HA-APOL3 with either GBP1, p62 (SQSTM1) or Galectin-8 at 2 h post infection (p.i). LPS-stained bacteria were not included in the merged image for clarity. Staining for endogenous Galectin-8 and p62 without IFN-γ; endogenous GBP1 with IFN-γ. (**B**) Targeting of APOL3^{mnGFP} to *Stm*^{RFP} in CRISPR-Cas9 HeLa cell lines lacking specific innate immune or autophagy pathways at 2 h p.i. Lines were deficient in GBP1 and GBP2; Galectin-3 or Galectin-8; TANK binding kinase-1 (TBK1); TNF receptor-associated factor 6 (TRAF6); Penta-KO lacking five autophagy cargo receptors (TAX1 binding protein 1 [TAX1BP1]; nuclear dot protein 52 kDa [NDP52/ CALCOCO2]; next to BRCA1 gene 1 protein

[NBR1], sequestrome 1 [SQSTM1/p62], and optineurin [OPTN]); HexaKO lacking six Atg8 family members (LC3A, LC3B, LC3C, GABARAP, GABARAPL1, and GABARAPL2). (**C**) *Stm* targeting by GBP1, Gal8, and p62 in wildtype or Δ*APOL3* HeLa cells at 2 h p.i. (**D**) Creation of doxycycline-inducible (Tet responsive element, TRE) HeLa cells expressing *APOL3*, *GBP1* or both in tandem separated by the self-cleavable P2A peptide. Whole cell lysates were proved by immunoblot 18 h after inducing with doxycycline (100 ng/ml). Data are mean ± s.e.m from 2 or 3 independent experiments (n = 100 bacteria counted for each condition) [(A) to (C)] and representative images are shown. ϕ, non-specific band. Scale bar 5 μm

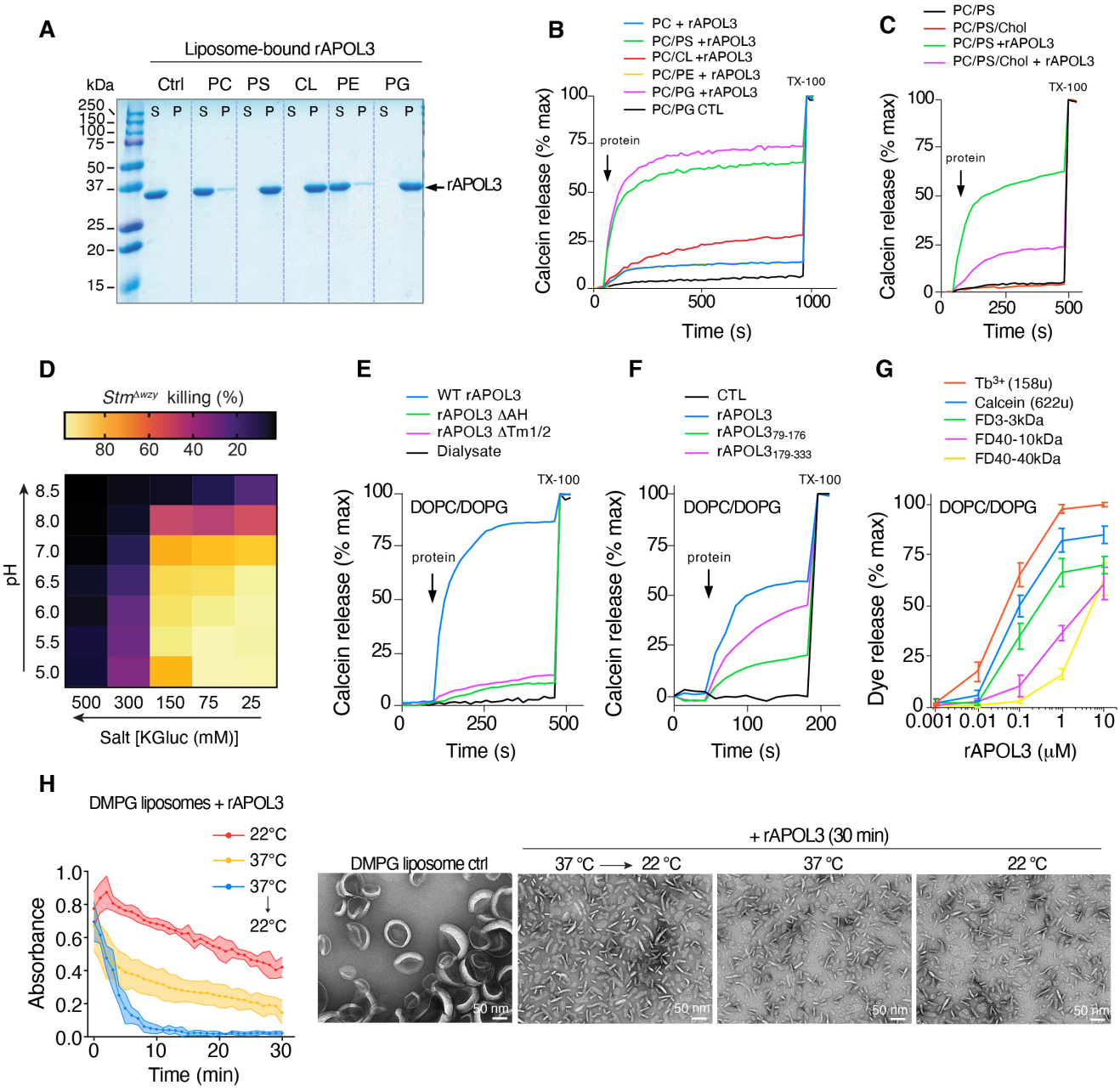

Fig. S11 Characterization of liposome permeabilization by rAPOL3. (**A** and **B**) Calcein loaded DOPC-based liposomes (0.5 mM) containing 20% of the indicated lipid were treated with rAPOL3 (500 nM). Liposome binding is indicated by SDS-PAGE and Coomassie blue staining of the supernatant (S) and pellet (P) following ultracentrifugation of liposome-APOL3 mixtures (A) and leakage was measured by increase in calcein fluorescence over time with 0.1% Triton-X100 added to achieve maximum leakage (B). (**C**) Calcein release from liposomes containing 25% cholesterol (chol) after addition of 200 nM rAPOL3. (**D**) Heatmap depiction of *Stm*$^{\Delta wzy}$ (single O-antigen unit) viability after treatment with 5 μM rAPOL3 (2 h) at 37°C across a gradient of salt (Potassium Gluconate) and pH. (**E** and **F**) Calcein release from liposomes treated with 500 nM of the indicated rAPOL3 mutant (E) or 200 nM of rAPOL3 fragment (F). (**G**) Different size fluorescent dyes were encapsulated in DOPC/DOPG liposomes and terminal dye release measured after treatment with

the indicated amount of rAPOL3 for 20 min. (**H**) Solubilization of DMPG liposomes (measured by a drop in absorbance at 400 nm) upon addition of rAPOL3 and incubated at the indicated temperature. Representative images of liposome mixtures by negative stain electron microscopy are shown after 30 min. Data from [(A) to (F]) are representative of 3 or 4 independent experiments. Data from [(G) and (H)] are mean ± s.d from 3 technical replicates representative of 2 independent experiments.

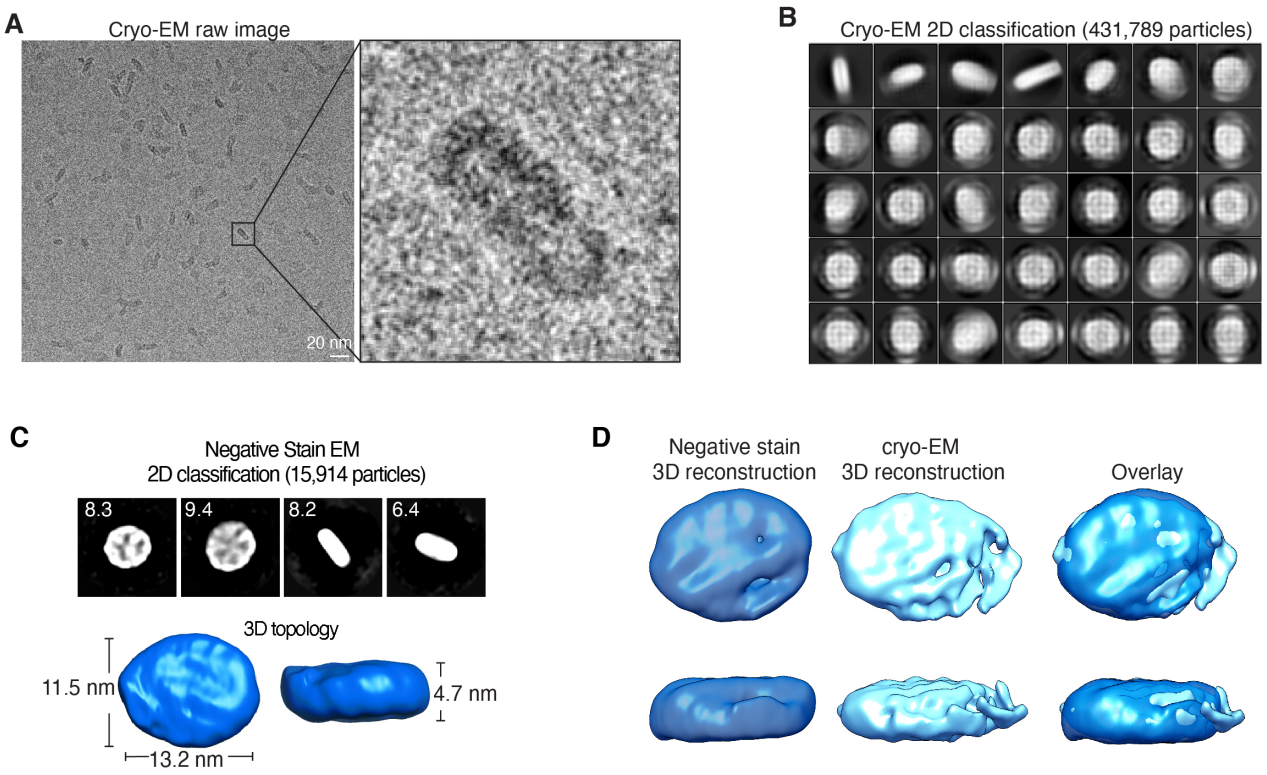

Fig. S12. Single-particle cryo-EM analysis of APOL3 lipoprotein nanodiscs. (**A**) Representative Cryo-EM micrograph of DMPC/DMPG liposomes 30 minutes after addition of rAPOL3. Side view of the APOL3 lipoprotein particle is highlighted. (**B**) 2D classification of particles selected for re-constructions depicted below. (**C**) 2D classification from negative stain-EM images of DMPC/DMPG liposomes 30 minutes after addition of rAPOL3. Percentage of each class indicated. Below are isosurface depictions of the top and side views of the 3D re-construction representing the most dominant particle. (**D**) Isosurface comparison of the dominant particle class re-constructed by negative stain-EM (dark blue) and Cryo-EM (light blue).

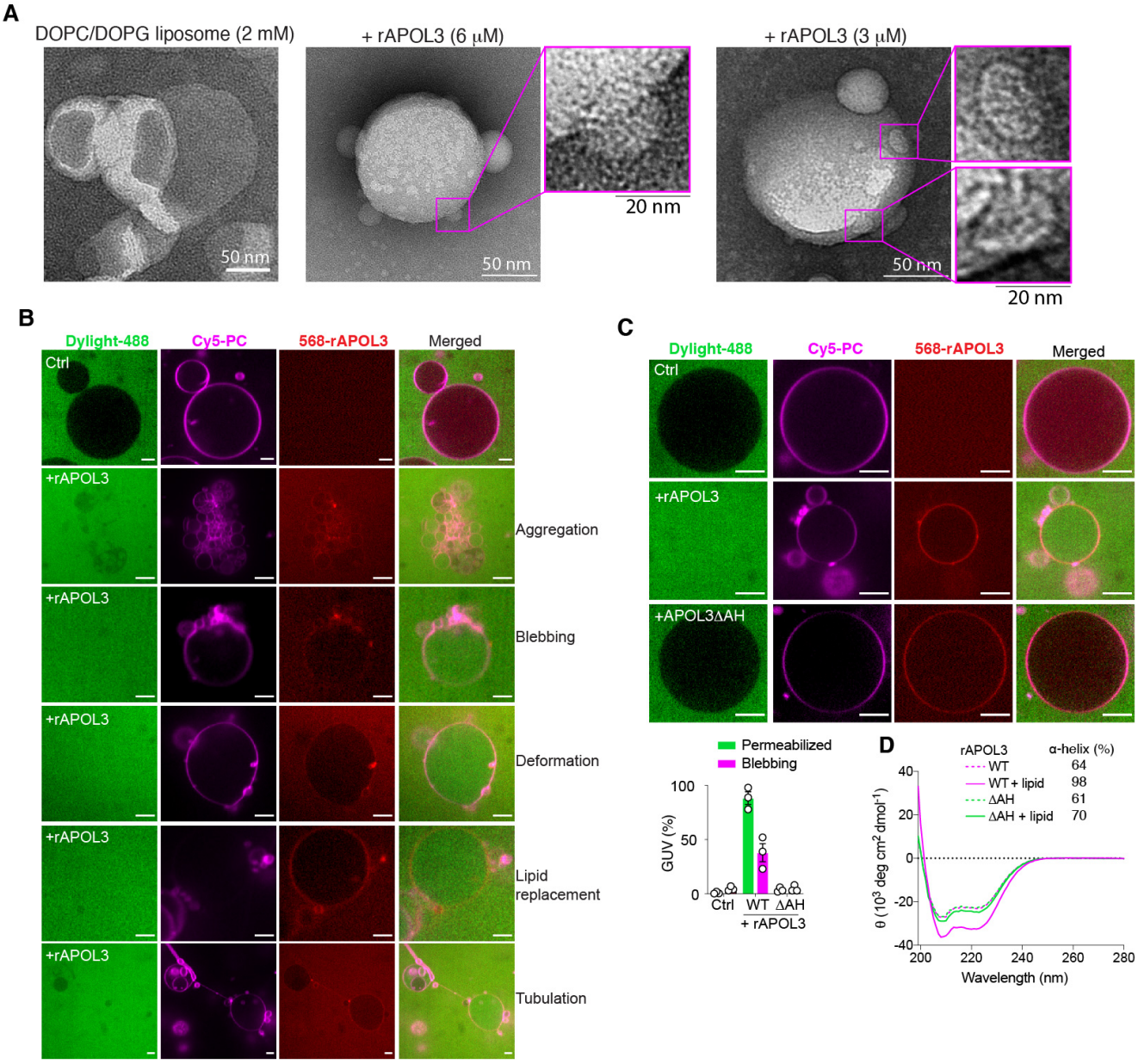

Fig. S13. APOL3 triggers pronounced membrane defects. (**A**) Negative stain EM micrographs of liposomes (DOPC:DOPG 80:20) before or immediately after addition of the indicated amount of rAPOL3. Inset images indicate APOL3-triggered membrane blebbing and lipid extraction. (**B**) Single plane confocal images of the observed membrane alteration after addition of 568-labelled rAPOL3 (300 nM) to Cy5-labelled giant unilamellar vesicles (GUVs). GUVs were composed of 80% DOPC and 20% DOPG and were incubated in soluble Dylight 488 to monitor permeability. (**C**) GUVs treated with 568-labelled WT or ΔAH rAPOL3 for 10 min prior to imaging. Shown are representative single plane confocal images and quantification (mean ± s.e.m from 3 independent experiments). (**D**) Circular dichroism spectra and estimated α-helical content of rAPOL3 variants in the presence or absence of PC/PG liposomes. Spectra are representative of 2 independent experiments. Scale bars 10 μm (B).

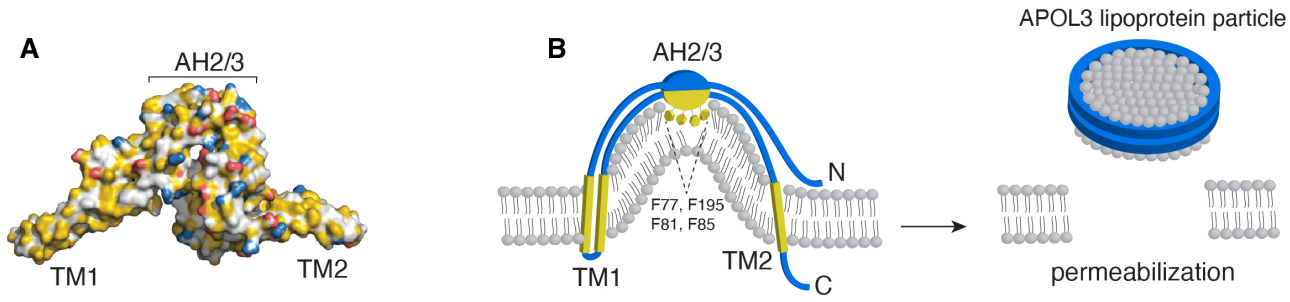

Fig. S14. Hypothetical model for membrane solubilization by APOL3. (**A**) Phyre2 predicted structure of APOL3 visualized with YRB lighting. Glu and Asp are red, and Arg and Lys are blue. All carbons not bound to nitrogen and oxygen are yellow. (**B**) Model for APOL3 lipid extraction based on predicted structure. AH2/3 insert the indicated 4 Phenylalanine residues to trigger positive curvature, permitting insertion of TM1 and 2 and formation of the APOL3 lipoprotein particle concomitant with membrane permeabilization.

Table S2 sgRNA sequences used in this study

Gene	sgRNA pool
APOL3(1)	5-CGCAGTCACGAATCTCTTCC-3 5-AGTGCTTTGACTCGTATACA-3
APOL3(2)	5-AATAACCAGACACGTTCTCC-3 5-GACTCTCTCCCGGAAGTATT-3
APOL1	5-GTGCAACAAAACGTTCCAAG-3 5-ACTCCTGCTGACTGATAATG-3 5-GATCCTCAAAGTAAGCCCCT-3 5-GCCAAGCTCACCAGATGCAG-3
APOL2	5-ACGAGCCCAAGCCCGCAACT-3 5-GGGGCATACGCTCCTAACTG-3 5-GCAGATTCTCTCTGCTCACT-3 5-AGCGAGCCTACCTGGGTTCA-3
APOL4	5-AGGCTGCGTCATCGCCAATG-3 5-TTGGACGCCCTTTGATTGCT-3 5-TGCTGACTAGCGATGAAGCC-3 5-TGCGTGTGGCTGAATTGCCC-3
APOL6	5-GACCAAAAATGCTCGCGTGC-3 5-TTTGCACCTGCACGCGGCTC-3 5-ACAGAGGCTGATGGACAACC-3 5-CCTCACTTTCTCTCTCCGCC-3
GBP1	5-TTTAGTGTGAGACTGCACCG-3 5-GTGCCCCACCCCAAGAAGCC-3
GBP2	5-CCTAGTTCTGCTCGACACTG-3
STAT1	5-TCCCATTACAGGCTCAGTCG-3 5-ATTGATCATCCAGCTGTGAC-3 5-TTCCCTATAGGATGTCTCAG-3 5-GCAGCTTGACTCAAAATTCC-3
Non-Targeting	5-ACGGAGGCTAAGCGTCGCAA-3 5-CGCTTCCGCGGCCCGTTCAA-3
LGALS3	5-CAGCTCCATGATGCGTTATC-3 5-CAGACCCAGATAACGCATCA-3
LGALS8	5-ATGTTCCTAGTGACGCAGAC-3 5-CGTATCACAATCAAAGTTCC-3
TBK1	5-TGGCTTTTATCTGATATTTT-3
TRAF6	5-TGTAGAGTTTGACCCACCCC-3 5-GCTGGAGAGGTTCCCCGTGC-3

Movie S1
Bacterial targeting by APOL3. HeLa cell expressing APOL3^{mnGFP} infected with *Stm*^{RFP}. Imaging was initiated 45 min post infection. Images are widefield maximum intensity projections from 5 μm stacks and were bleach corrected using Fiji.

Movie S2
APOL3 mobilization by sterile endosomal damage. HeLa cell expressing APOL3^{mnGFP} imaged immediately after triggering endosomal damage with 1 mM LLOMe. Images are widefield maximum intensity projections from 5 μm stacks and were bleach corrected using Fiji.

Movie S3
Stm* IM damage triggered by APOL3 *in situ. IFN-γ treated HeLa cell expressing APOL3^{RFP} and infected with *Stm*-minD^{mnGFP} initiated 45 min post infection. Image is a widefield maximum intensity projection from 5 μm stacks and was bleach corrected using Fiji. Constitutive minD^{mnGFP} expression (used here) results in elongated *Stm*.

Movie S4
Stm* IM damage triggered by APOL3 *in situ. A second example of an IFN-γ treated HeLa cell expressing APOL3^{RFP} and infected with *Stm*-minD^{mnGFP} initiated 45 min post infection. Image is a widefield maximum intensity projection from 5 μm stacks and was bleach corrected using Fiji. Constitutive minD^{mnGFP} expression (used here) results in elongated *Stm*.

Movie S5
Bacterial penetration of APOL3 in IFN-γ activated cells. 360°C rotation of a 3D surface rendering (Fig. 2f) generated from structured illumination microscopy (SIM) of immunolabeled HA-APOL3 and LPS 150 min post infection in IFN-γ activated cells.

Movie S6
Clearance of APOL3 targeted bacteria from IFN-γ activated cells. IFN-γ treated HeLa cell expressing APOL3^{mnGFP} and infected with *Stm*^{RFP}. Images are widefield maximum intensity projections from 5 μm stacks and were bleach corrected using Fiji. APOL3 coated bacteria (denoted by arrows in first frame) fade from view whereas untargeted bacteria persist.

Movie S7
Stm* IM damage triggered by APOL3 *in vitro. *Stm* expressing minD^{mnGFP} were extracted from LLOMe-treated IFN-γ activated Δ*APOL3* cells and treated as mock control. Bacteria were immobilized on agarose pads and wide-field imaging initiated after ~2 min. Images were taken every 12 seconds. scale bar 2 μm.

Movie S8
Stm* IM damage triggered by APOL3 *in vitro. *Stm* expressing minD^{mnGFP} were extracted from LLOMe-treated IFN-γ activated Δ*APOL3* cells and treated with CCCP – a known disrupter of IM membrane potential. Bacteria were immobilized on agarose pads and wide-field imaging initiated after ~2 min. Images were taken every 12 seconds. scale bar 2 μm.

Movie S9

***Stm* IM damage triggered by APOL3 *in vitro*.** *Stm* expressing minD^{mnGFP} were extracted from LLOMe-treated IFN-γ activated Δ*APOL3* cells and treated with 5 μM rAPOL3. Bacteria were immobilized on agarose pads and wide-field imaging initiated after ~2 min. Images were taken every 12 seconds. scale bar 2 μm.

Movie S10

Permeation of GUVs by APOL3. Single plane from confocal microscopy of GUV's composed of DOPC/DOPG (80:20) incubated in Dylight™ 488 free acid (indicator of permeability) were treated with 568-labelled rAPOL3 and imaged live. See movie S11 for 568-rAPOL3 channel alone. Arrow indicates rAPOL3-triggered membrane blebbing occurring concomitantly with GUV permeabilization.

Movie S11

Permeation of GUVs by APOL3. Single plane from confocal microscopy (GUVs described in movie S10) showing the 568-rAPOL3 channel alone.

Table S1

Genome-wide CRISPR/Cas9 screen and RNAseq results. Shown are gene-level MAGeCK *P* values depicting enrichment in H^R versus S^R FACS sorted *Stm*-infected HeLa cells in the presence or absence of IFN-γ. RNAseq analysis depicting the fold induction (relative to untreated) of each gene in the presence of IFN-γ and *Stm* is also shown.

References

1. F. Randow, J. D. MacMicking, L. C. James, Cellular self-defense: How cell-autonomous immunity protects against pathogens. *Science* **340**, 701–706 (2013). doi:10.1126/science.1233028 Medline

2. J. D. MacMicking, Interferon-inducible effector mechanisms in cell-autonomous immunity. *Nat. Rev. Immunol.* **12**, 367–382 (2012). doi:10.1038/nri3210 Medline

3. K. Schroder, P. J. Hertzog, T. Ravasi, D. A. Hume, Interferon-γ: An overview of signals, mechanisms and functions. *J. Leukoc. Biol.* **75**, 163–189 (2004). doi:10.1189/jlb.0603252 Medline

4. S.-Y. Zhang, S. Boisson-Dupuis, A. Chapgier, K. Yang, J. Bustamante, A. Puel, C. Picard, L. Abel, E. Jouanguy, J.-L. Casanova, Inborn errors of interferon (IFN)-mediated immunity in humans: Insights into the respective roles of IFN-α/β, IFN-γ, and IFN-λ in host defense. *Immunol. Rev.* **226**, 29–40 (2008). doi:10.1111/j.1600-065X.2008.00698.x Medline

5. S.-Y. Zhang, E. Jouanguy, Q. Zhang, L. Abel, A. Puel, J.-L. Casanova, Human inborn errors of immunity to infection affecting cells other than leukocytes: From the immune system to the whole organism. *Curr. Opin. Immunol.* **59**, 88–100 (2019). doi:10.1016/j.coi.2019.03.008 Medline

6. T. Krausgruber, N. Fortelny, V. Fife-Gernedl, M. Senekowitsch, L. C. Schuster, A. Lercher, A. Nemc, C. Schmidl, A. F. Rendeiro, A. Bergthaler, C. Bock, Structural cells are key regulators of organ-specific immune responses. *Nature* **583**, 296–302 (2020). doi:10.1038/s41586-020-2424-4 Medline

7. L. A. Knodler, B. A. Vallance, J. Celli, S. Winfree, B. Hansen, M. Montero, O. Steele-Mortimer, Dissemination of invasive Salmonella via bacterial-induced extrusion of mucosal epithelia. *Proc. Natl. Acad. Sci. U.S.A.* **107**, 17733–17738 (2010). doi:10.1073/pnas.1006098107 Medline

8. C. R. Beuzón, S. Méresse, K. E. Unsworth, J. Ruíz-Albert, S. Garvis, S. R. Waterman, T. A. Ryder, E. Boucrot, D. W. Holden, Salmonella maintains the integrity of its intracellular vacuole through the action of SifA. *EMBO J.* **19**, 3235–3249 (2000). doi:10.1093/emboj/19.13.3235 Medline

9. M. Chen, H. Sun, M. Boot, L. Shao, S.-J. Chang, W. Wang, T. T. Lam, M. Lara-Tejero, E. H. Rego, J. E. Galán, Itaconate is an effector of a Rab GTPase cell-autonomous host defense pathway against *Salmonella*. *Science* **369**, 450–455 (2020). doi:10.1126/science.aaz1333 Medline

10. E. E. Smith, H. S. Malik, The apolipoprotein L family of programmed cell death and immunity genes rapidly evolved in primates at discrete sites of host-pathogen interactions. *Genome Res.* **19**, 850–858 (2009). doi:10.1101/gr.085647.108 Medline

11. L. Vanhamme, F. Paturiaux-Hanocq, P. Poelvoorde, D. P. Nolan, L. Lins, J. Van Den Abbeele, A. Pays, P. Tebabi, H. Van Xong, A. Jacquet, N. Moguilevsky, M. Dieu, J. P. Kane, P. De Baetselier, R. Brasseur, E. Pays, Apolipoprotein L-I is the trypanosome lytic factor of human serum. *Nature* **422**, 83–87 (2003). doi:10.1038/nature01461 Medline

12. D. Pérez-Morga, B. Vanhollebeke, F. Paturiaux-Hanocq, D. P. Nolan, L. Lins, F. Homblé, L. Vanhamme, P. Tebabi, A. Pays, P. Poelvoorde, A. Jacquet, R. Brasseur, E. Pays, Apolipoprotein L-I promotes trypanosome lysis by forming pores in lysosomal membranes. *Science* **309**, 469–472 (2005). doi:10.1126/science.1114566 Medline

13. T. L. M. Thurston, M. P. Wandel, N. von Muhlinen, A. Foeglein, F. Randow, Galectin 8 targets damaged vesicles for autophagy to defend cells against bacterial invasion. *Nature* **482**, 414–418 (2012). doi:10.1038/nature10744 Medline

14. H. Strahl, L. W. Hamoen, Membrane potential is important for bacterial cell division. *Proc. Natl. Acad. Sci. U.S.A.* **107**, 12281–12286 (2010). doi:10.1073/pnas.1005485107 Medline

15. F. Fontaine, L. Lecordier, G. Vanwalleghem, P. Uzureau, N. Van Reet, M. Fontaine, P. Tebabi, B. Vanhollebeke, P. Büscher, D. Pérez-Morga, E. Pays, APOLs with low pH dependence can kill all African trypanosomes. *Nat. Microbiol.* **2**, 1500–1506 (2017). doi:10.1038/s41564-017-0034-1 Medline

16. T. Miki, W.-D. Hardt, Outer membrane permeabilization is an essential step in the killing of gram-negative bacteria by the lectin RegIIIβ. *PLOS ONE* **8**, e69901 (2013). doi:10.1371/journal.pone.0069901 Medline

17. R. L. Gallo, L. V. Hooper, Epithelial antimicrobial defence of the skin and intestine. *Nat. Rev. Immunol.* **12**, 503–516 (2012). doi:10.1038/nri3228 Medline

18. Y. T. Zheng, S. Shahnazari, A. Brech, T. Lamark, T. Johansen, J. H. Brumell, The adaptor protein p62/SQSTM1 targets invading bacteria to the autophagy pathway. *J. Immunol.* **183**, 5909–5916 (2009). doi:10.4049/jimmunol.0900441 Medline

19. B.-H. Kim, A. R. Shenoy, P. Kumar, R. Das, S. Tiwari, J. D. MacMicking, A family of IFN-γ-inducible 65-kD GTPases protects against bacterial infection. *Science* **332**, 717–721 (2011). doi:10.1126/science.1201711 Medline

20. B.-H. Kim, J. D. Chee, C. J. Bradfield, E.-S. Park, P. Kumar, J. D. MacMicking, Interferon-induced guanylate-binding proteins in inflammasome activation and host defense. *Nat. Immunol.* **17**, 481–489 (2016). doi:10.1038/ni.3440 Medline

21. A. R. Shenoy, D. A. Wellington, P. Kumar, H. Kassa, C. J. Booth, P. Cresswell, J. D. MacMicking, GBP5 promotes NLRP3 inflammasome assembly and immunity in mammals. *Science* **336**, 481–485 (2012). doi:10.1126/science.1217141 Medline

22. M. P. Wandel, B.-H. Kim, E.-S. Park, K. B. Boyle, K. Nayak, B. Lagrange, A. Herod, T. Henry, M. Zilbauer, J. Rohde, J. D. MacMicking, F. Randow, Guanylate-binding proteins convert cytosolic bacteria into caspase-4 signaling platforms. *Nat. Immunol.* **21**, 880–891 (2020). doi:10.1038/s41590-020-0697-2 Medline

23. J. C. Santos, D. Boucher, L. K. Schneider, B. Demarco, M. Dilucca, K. Shkarina, R. Heilig, K. W. Chen, R. Y. H. Lim, P. Broz, Human GBP1 binds LPS to initiate assembly of a caspase-4 activating platform on cytosolic bacteria. *Nat. Commun.* **11**, 3276 (2020). doi:10.1038/s41467-020-16889-z Medline

24. M. Kutsch, L. Sistemich, C. F. Lesser, M. B. Goldberg, C. Herrmann, J. Coers, Direct binding of polymeric GBP1 to LPS disrupts bacterial cell envelope functions. *EMBO J.* **39**, e104926 (2020). doi:10.15252/embj.2020104926 Medline

25. T. H. Bayburt, Y. V. Grinkova, S. G. Sligar, Self-Assembly of Discoidal Phospholipid Bilayer Nanoparticles with Membrane Scaffold Proteins. *Nano Lett.* **2**, 853–856 (2002). doi:10.1021/nl025623k

26. W. K. Surewicz, R. M. Epand, H. J. Pownall, S. W. Hui, Human apolipoprotein A-I forms thermally stable complexes with anionic but not with zwitterionic phospholipids. *J. Biol. Chem.* **261**, 16191–16197 (1986). doi:10.1016/S0021-9258(18)66697-9 Medline

27. K. Gupta, J. Li, I. Liko, J. Gault, C. Bechara, D. Wu, J. T. S. Hopper, K. Giles, J. L. P. Benesch, C. V. Robinson, Identifying key membrane protein lipid interactions using mass spectrometry. *Nat. Protoc.* **13**, 1106–1120 (2018). doi:10.1038/nprot.2018.014 Medline

28. K. Gupta, J. A. C. Donlan, J. T. S. Hopper, P. Uzdavinys, M. Landreh, W. B. Struwe, D. Drew, A. J. Baldwin, P. J. Stansfeld, C. V. Robinson, The role of interfacial lipids in stabilizing membrane protein oligomers. *Nature* **541**, 421–424 (2017). doi:10.1038/nature20820 Medline

29. J. E. Keener, D. E. Zambrano, G. Zhang, C. K. Zak, D. J. Reid, B. S. Deodhar, J. E. Pemberton, J. S. Prell, M. T. Marty, Chemical additives enable native mass spectrometry measurement of membrane protein oligomeric state within intact nanodiscs. *J. Am. Chem. Soc.* **141**, 1054–1061 (2019). doi:10.1021/jacs.8b11529 Medline

30. J. M. Stokes, C. R. MacNair, B. Ilyas, S. French, J.-P. Côté, C. Bouwman, M. A. Farha, A. O. Sieron, C. Whitfield, B. K. Coombes, E. D. Brown, Pentamidine sensitizes Gram-negative pathogens to antibiotics and overcomes acquired colistin resistance. *Nat. Microbiol.* **2**, 17028 (2017). doi:10.1038/nmicrobiol.2017.28 Medline

31. M. Vaara, Polymyxins and Their Potential Next Generation as Therapeutic Antibiotics. *Front. Microbiol.* **10**, 1689 (2019). doi:10.3389/fmicb.2019.01689 Medline

32. T. Clairfeuille, K. R. Buchholz, Q. Li, E. Verschueren, P. Liu, D. Sangaraju, S. Park, C. L. Noland, K. M. Storek, N. N. Nickerson, L. Martin, T. Dela Vega, A. Miu, J. Reeder, M. Ruiz-Gonzalez, D. Swem, G. Han, D. P. DePonte, M. S. Hunter, C. Gati, S. Shahidi-Latham, M. Xu, N. Skelton, B. D. Sellers, E. Skippington, W. Sandoval, E. J. Hanan, J. Payandeh, S. T. Rutherford, Structure of the essential inner membrane lipopolysaccharide-PbgA complex. *Nature* **584**, 479–483 (2020). doi:10.1038/s41586-020-2597-x Medline

33. K. A. Brogden, Antimicrobial peptides: Pore formers or metabolic inhibitors in bacteria? *Nat. Rev. Microbiol.* **3**, 238–250 (2005). doi:10.1038/nrmicro1098 Medline

34. N. Mookherjee, M. A. Anderson, H. P. Haagsman, D. J. Davidson, Antimicrobial host defence peptides: Functions and clinical potential. *Nat. Rev. Drug Discov.* **19**, 311–332 (2020). doi:10.1038/s41573-019-0058-8 Medline

35. C. Sohlenkamp, O. Geiger, Bacterial membrane lipids: Diversity in structures and pathways. *FEMS Microbiol. Rev.* **40**, 133–159 (2016). doi:10.1093/femsre/fuv008 Medline

36. W. A. Ernst, S. Thoma-Uszynski, R. Teitelbaum, C. Ko, D. A. Hanson, C. Clayberger, A. M. Krensky, M. Leippe, B. R. Bloom, T. Ganz, R. L. Modlin, Granulysin, a T cell product, kills bacteria by altering membrane permeability. *J. Immunol.* **165**, 7102–7108 (2000). doi:10.4049/jimmunol.165.12.7102 Medline

37. H. Barman, M. Walch, S. Latinovic-Golic, C. Dumrese, M. Dolder, P. Groscurth, U. Ziegler, Cholesterol in negatively charged lipid bilayers modulates the effect of the antimicrobial protein granulysin. *J. Membr. Biol.* **212**, 29–39 (2006). doi:10.1007/s00232-006-0040-3 Medline

38. S. Stenger, D. A. Hanson, R. Teitelbaum, P. Dewan, K. R. Niazi, C. J. Froelich, T. Ganz, S. Thoma-Uszynski, A. Melián, C. Bogdan, S. A. Porcelli, B. R. Bloom, A. M. Krensky, R. L. Modlin, An antimicrobial activity of cytolytic T cells mediated by granulysin. *Science* **282**, 121–125 (1998). doi:10.1126/science.282.5386.121 Medline

39. G. van Meer, D. R. Voelker, G. W. Feigenson, Membrane lipids: Where they are and how they behave. *Nat. Rev. Mol. Cell Biol.* **9**, 112–124 (2008). doi:10.1038/nrm2330 Medline

40. A. Rausell, Y. Luo, M. Lopez, Y. Seeleuthner, F. Rapaport, A. Favier, P. D. Stenson, D. N. Cooper, E. Patin, J.-L. Casanova, L. Quintana-Murci, L. Abel, Common homozygosity for predicted loss-of-function variants reveals both redundant and advantageous effects of dispensable human genes. *Proc. Natl. Acad. Sci. U.S.A.* **117**, 13626–13636 (2020). doi:10.1073/pnas.1917993117 Medline

41. R. G. Gaudet, C. J. Bradfield, J. D. MacMicking, Evolution of Cell-Autonomous Effector Mechanisms in Macrophages versus Non-Immune Cells. *Microbiol. Spectr.* **4**, 10.1128/microbiolspec.MCHD-0050-2016 (2016). doi:10.1128/microbiolspec.MCHD-0050-2016 Medline

42. L. Kamareddine, J. Nakhleh, M. A. Osta, Functional Interaction between Apolipophorins and Complement Regulate the Mosquito Immune Response to Systemic Infections. *J. Innate Immun.* **8**, 314–326 (2016). doi:10.1159/000443883 Medline

43. A. Zdybicka-Barabas, M. Cytryńska, Involvement of apolipophorin III in antibacterial defense of Galleria mellonella larvae. *Comp. Biochem. Physiol. B* **158**, 90–98 (2011). doi:10.1016/j.cbpb.2010.10.001 Medline

44. R. Figueira, K. G. Watson, D. W. Holden, S. Helaine, Identification of salmonella pathogenicity island-2 type III secretion system effectors involved in intramacrophage replication of S. enterica serovar typhimurium: Implications for rational vaccine design. *mBio* **4**, e00065 (2013). doi:10.1128/mBio.00065-13 Medline

45. S. Helaine, A. M. Cheverton, K. G. Watson, L. M. Faure, S. A. Matthews, D. W. Holden, Internalization of Salmonella by macrophages induces formation of nonreplicating persisters. *Science* **343**, 204–208 (2014). doi:10.1126/science.1244705 Medline

46. A. J. Karlsson, H.-K. Lim, H. Xu, M. A. Rocco, M. A. Bratkowski, A. Ke, M. P. DeLisa, Engineering antibody fitness and function using membrane-anchored display of correctly folded proteins. *J. Mol. Biol.* **416**, 94–107 (2012). doi:10.1016/j.jmb.2011.12.021 Medline

47. Y. Chao, J. Vogel, A 3′ UTR-Derived Small RNA Provides the Regulatory Noncoding Arm of the Inner Membrane Stress Response. *Mol. Cell* **61**, 352–363 (2016). doi:10.1016/j.molcel.2015.12.023 Medline

48. R. G. Gaudet, A. Sintsova, C. M. Buckwalter, N. Leung, A. Cochrane, J. Li, A. D. Cox, J. Moffat, S. D. Gray-Owen, Cytosolic detection of the bacterial metabolite HBP activates TIFA-dependent innate immunity. *Science* **348**, 1251–1255 (2015). doi:10.1126/science.aaa4921 Medline

49. Q. Kong, J. Yang, Q. Liu, P. Alamuri, K. L. Roland, R. Curtiss 3rd, Effect of deletion of genes involved in lipopolysaccharide core and O-antigen synthesis on virulence and immunogenicity of Salmonella enterica serovar typhimurium. *Infect. Immun.* **79**, 4227–4239 (2011). doi:10.1128/IAI.05398-11 Medline

50. M. Lazarou, D. A. Sliter, L. A. Kane, S. A. Sarraf, C. Wang, J. L. Burman, D. P. Sideris, A. I. Fogel, R. J. Youle, The ubiquitin kinase PINK1 recruits autophagy receptors to induce mitophagy. *Nature* **524**, 309–314 (2015). doi:10.1038/nature14893 Medline

51. T. N. Nguyen, B. S. Padman, J. Usher, V. Oorschot, G. Ramm, M. Lazarou, Atg8 family LC3/GABARAP proteins are crucial for autophagosome-lysosome fusion but not autophagosome formation during PINK1/Parkin mitophagy and starvation. *J. Cell Biol.* **215**, 857–874 (2016). doi:10.1083/jcb.201607039 Medline

52. O. Shalem, N. E. Sanjana, E. Hartenian, X. Shi, D. A. Scott, T. Mikkelson, D. Heckl, B. L. Ebert, D. E. Root, J. G. Doench, F. Zhang, Genome-scale CRISPR-Cas9 knockout

screening in human cells. *Science* **343**, 84–87 (2014). doi:10.1126/science.1247005 Medline

53. W. Li, H. Xu, T. Xiao, L. Cong, M. I. Love, F. Zhang, R. A. Irizarry, J. S. Liu, M. Brown, X. S. Liu, MAGeCK enables robust identification of essential genes from genome-scale CRISPR/Cas9 knockout screens. *Genome Biol.* **15**, 554 (2014). doi:10.1186/s13059-014-0554-4 Medline

54. C. Wiedemann, P. Bellstedt, M. Görlach, CAPITO—A web server-based analysis and plotting tool for circular dichroism data. *Bioinformatics* **29**, 1750–1757 (2013). doi:10.1093/bioinformatics/btt278 Medline

55. J. Zivanov, T. Nakane, B. O. Forsberg, D. Kimanius, W. J. Hagen, E. Lindahl, S. H. Scheres, New tools for automated high-resolution cryo-EM structure determination in RELION-3. *eLife* **7**, e42166 (2018). doi:10.7554/eLife.42166 Medline

56. J. R. Gallagher, A. J. Kim, N. M. Gulati, A. K. Harris, Negative-Stain Transmission Electron Microscopy of Molecular Complexes for Image Analysis by 2D Class Averaging. *Curr. Protoc. Microbiol.* **54**, e90 (2019). doi:10.1002/cpmc.90 Medline

57. S. Q. Zheng, E. Palovcak, J.-P. Armache, K. A. Verba, Y. Cheng, D. A. Agard, MotionCor2: Anisotropic correction of beam-induced motion for improved cryo-electron microscopy. *Nat. Methods* **14**, 331–332 (2017). doi:10.1038/nmeth.4193 Medline

58. K. Zhang, Gctf: Real-time CTF determination and correction. *J. Struct. Biol.* **193**, 1–12 (2016). doi:10.1016/j.jsb.2015.11.003 Medline

59. E. F. Pettersen, T. D. Goddard, C. C. Huang, G. S. Couch, D. M. Greenblatt, E. C. Meng, T. E. Ferrin, UCSF Chimera—A visualization system for exploratory research and analysis. *J. Comput. Chem.* **25**, 1605–1612 (2004). doi:10.1002/jcc.20084 Medline

60. R. Gautier, D. Douguet, B. Antonny, G. Drin, HELIQUEST: A web server to screen sequences with specific α-helical properties. *Bioinformatics* **24**, 2101–2102 (2008). doi:10.1093/bioinformatics/btn392 Medline

61. L. A. Kelley, S. Mezulis, C. M. Yates, M. N. Wass, M. J. E. Sternberg, The Phyre2 web portal for protein modeling, prediction and analysis. *Nat. Protoc.* **10**, 845–858 (2015). doi:10.1038/nprot.2015.053 Medline

62. D. Hagemans, I. A. E. M. van Belzen, T. Morán Luengo, S. G. D. Rüdiger, A script to highlight hydrophobicity and charge on protein surfaces. *Front. Mol. Biosci.* **2**, 56 (2015). doi:10.3389/fmolb.2015.00056 Medline